

Spin-Imbalanced Pairing and Fermi Surface Deformation in Flat Bands

Kukka-Emilia Huhtinen,* Marek Tylutki,* Pramod Kumar, Tuomas I. Vanhala, Sebastiano Peotta, and Päivi Törmä†
Department of Applied Physics, Aalto University, 00076 Aalto, Finland

(Dated: June 13, 2018)

We study the attractive Hubbard model with spin imbalance on two lattices featuring a flat band: the Lieb and kagome lattices. We present mean-field phase diagrams featuring exotic superfluid phases, similar to the Fulde-Ferrell-Larkin-Ovchinnikov (FFLO) state, whose stability is confirmed by dynamical mean-field theory (DMFT). The nature of the pairing is found to be richer than just the Fermi surface shift responsible for the usual FFLO state. The presence of a flat band allows for changes in the particle momentum distributions at null energy cost. This facilitates formation of nontrivial superfluid phases via multiband Cooper pair formation: the momentum distribution of the spin component in the flat band deforms to mimic the Fermi surface of the other spin component residing in a dispersive band. The Fermi surface of the unpaired particles that are typical for gapless superfluids becomes deformed as well. The results highlight the profound effect of flat dispersions on Fermi surface instabilities, and provide a potential route for observing spin-imbalanced superfluidity and superconductivity.

I. INTRODUCTION

Interactions in fermion systems may cause Fermi surface (FS) instabilities, for instance towards pairing¹ or symmetry-breaking deformations of the FS, called the Pomeranchuk instability (PI)². These mechanisms lead to various phases of matter such as both conventional and high- T_c superconductivity³⁻⁵, topological phases thereof⁶, the two superfluid phases of different symmetry in ³He⁷ or superfluidity in lattice systems of ultracold fermions predicted by the Hubbard model⁸, including models with spin-orbit coupling^{9,10}. In the repulsive Hubbard model, the superfluidity may coexist with the magnetic stripe order¹¹, or with PI as in Refs.^{12,13}. Spin-imbalanced superfluidity, on the other hand, has been predicted to simultaneously display pairing, superfluidity, and gapless excitations (FSs). These exotic phases of matter spontaneously break symmetries of the system, for instance rotational or translational, in addition to the breaking of the $U(1)$ gauge symmetry characteristic of any BCS-type superfluid. In the FFLO state^{14,15} the Cooper pairs carry a finite momentum. Deformed FS superfluidity (DFS)^{16,17} has been proposed as another alternative that gives a lower energy than the conventional BCS theory. Such predictions have remained elusive, supported only by indirect experimental evidence^{18,19}. Phase separation, instead of exotic spin-imbalanced superfluids, has been observed in ultracold quantum gases²⁰⁻²⁴; this is consistent with predictions for continuum systems²⁵⁻²⁷, although theory suggests that lattice systems may stabilize the FFLO state due to nesting²⁸⁻³³. In general, singularities in the density of states (DOS) are known to enhance FS instabilities. Here we show that multiband lattice systems which possess the ultimate DOS singularity, namely a flat (constant) energy band, allow deformations of the particle momentum distribution without energy cost and thereby stabilize a new type of spin-imbalanced superfluidity. We find that the origin of the pairing is different from a simple minority particle FS shift

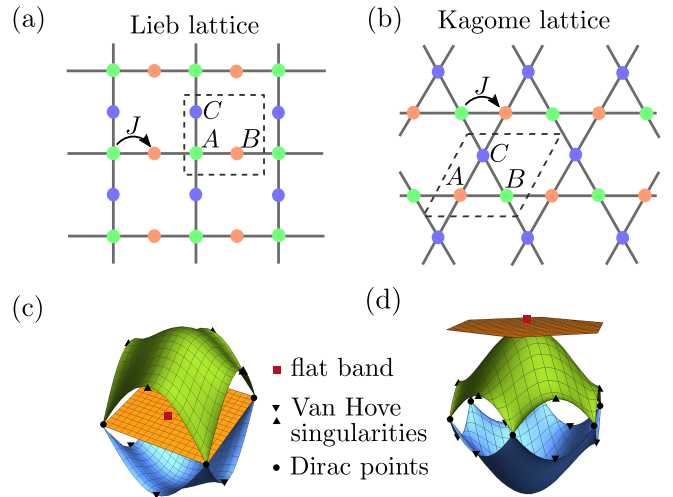


FIG. 1: Two lattice geometries featuring a FB: (a) a Lieb lattice and (b) a kagome lattice. The elementary cells are delimited with dashed lines. Three sites that constitute an elementary cell are labeled as A, B and C. Below, single-particle band structures of these lattices: (c) Lieb and (d) kagome with two dispersive bands and one FB. The singularities and Dirac points are shown in Fig. 2 with lines.

conventionally responsible for FFLO states.

II. MODEL

We study two examples of a Hubbard model with a flat band (FB) in the single-particle energy spectrum: a Lieb lattice and a kagome lattice Hubbard model. Both lattices have three sub-lattices and feature two dispersive bands and a FB,

$$E_{\pm, \text{Lb}}(\mathbf{k}) = \pm J \sqrt{2} \sqrt{2 + \cos k_x + \cos k_y}, \quad E_{\text{FB, Lb}} = 0 \quad (1)$$

$$E_{\pm, \text{Kg}}(\mathbf{k}) = J(1 \pm \sqrt{3 + 2\Lambda(\mathbf{k})}), \quad E_{\text{FB, Kg}} = 2J, \quad (2)$$

where $\Lambda(\mathbf{k}) = \sum_{i=1}^3 \cos(\mathbf{k} \cdot \mathbf{a}_i)$. The vectors \mathbf{a}_1 and \mathbf{a}_2 are the primitive vectors of the kagome lattice, and $\mathbf{a}_3 = \mathbf{a}_1 - \mathbf{a}_2$.

*These authors contributed equally to this work.

†Electronic address: paivi.torma@aalto.fi

The indices Lb and Kg refer to the Lieb and kagome lattices respectively. By J , which we also use as the unit of energy, we denote the hopping strength between the neighboring lattice sites. Hereafter the lattice constant a is assumed $a = 1$.

The lattices and the band structures are shown in Fig 1. Importantly, such lattices have been experimentally realized for ultracold gases^{34–36}, in designer lattices made by atomistic control^{37,38}, in optical analogues^{39,40} and also implementations with superconducting circuits have been proposed theoretically⁴¹. We choose to fix chemical potentials and therefore consider the grand-canonical ensemble. The real-space grand-canonical Hamiltonian reads

$$H = \sum_{\sigma} \sum_{i\alpha, j\beta} \psi_{i\alpha\sigma}^{\dagger} \mathcal{H}_{i\alpha, j\beta} \psi_{j\beta\sigma} - \sum_{\sigma} \mu_{\sigma} N_{\sigma} + H_{\text{int}}, \quad (3)$$

where the lattice information is contained in the single-particle Hamiltonian $\mathcal{H}_{i\alpha, j\beta}$ responsible for hopping between the lattice sites, α and β are the sublattice (orbital) indices. In our model, we consider only nearest neighbor hopping for both lattices. The particle number operator is defined as $N_{\sigma} = \sum_{i\alpha} \psi_{i\alpha\sigma}^{\dagger} \psi_{i\alpha\sigma}$, and the on-site interaction enters as $H_{\text{int}} = U \sum_{i\alpha} \psi_{i\alpha\uparrow}^{\dagger} \psi_{i\alpha\downarrow}^{\dagger} \psi_{i\alpha\downarrow} \psi_{i\alpha\uparrow}$. We define the average chemical potential as $\mu = (\mu_{\uparrow} + \mu_{\downarrow})/2$ and the effective magnetic field as $h = (\mu_{\uparrow} - \mu_{\downarrow})/2$.

The BCS (mean-field) approximation of the Hamiltonian (3) introduces a pairing field $\Delta_{i\alpha} = U \langle \psi_{i\alpha\downarrow} \psi_{i\alpha\uparrow} \rangle$, where the average denotes a ground state expectation value at zero temperature and a grand-canonical average at finite temperatures $k_B T = 1/\beta$. We allow for an imbalance in chemical potentials, $\mu_{\uparrow} \neq \mu_{\downarrow}$, so the particles in a Cooper pair may have a nonzero center-of-mass momentum \mathbf{q} . This is reflected by the Fulde-Ferrell (FF) ansatz for the pairing field, $\Delta_{j\alpha} = \Delta_{\alpha} e^{i\mathbf{q} \cdot \mathbf{j}}$. Since we assume our system to be translationally invariant, we change the basis to the quasi-momentum basis by performing a Fourier transform. After this transformation the mean-field Hamiltonian with the FF ansatz becomes

$$H_{\text{FF}} = \sum_{\mathbf{k}} \left[\Psi_{\mathbf{k}}^{\dagger} \mathcal{H}_{\text{BdG}} \Psi_{\mathbf{k}} - 3\mu_{\downarrow} - \frac{1}{U} \text{Tr} \Delta^{\dagger} \Delta \right], \quad (4)$$

where we introduced a Nambu spinor $\Psi_{\mathbf{k}} = (c_{\mathbf{k}, A\uparrow}, c_{\mathbf{k}, B\uparrow}, c_{\mathbf{k}, C\uparrow}, c_{\mathbf{q}-\mathbf{k}, A\downarrow}^{\dagger}, c_{\mathbf{q}-\mathbf{k}, B\downarrow}^{\dagger}, c_{\mathbf{q}-\mathbf{k}, C\downarrow}^{\dagger})^T$ and the Bogoliubov-de-Gennes (BdG) Hamiltonian

$$\mathcal{H}_{\text{BdG}} = \begin{pmatrix} \mathcal{H}_{\mathbf{k}} - \mu_{\uparrow} & \Delta \\ \Delta^{\dagger} & -\mathcal{H}_{-\mathbf{k}+\mathbf{q}} + \mu_{\downarrow} \end{pmatrix}. \quad (5)$$

The pairing fields are collected into a diagonal matrix $(\Delta)_{\alpha\beta} = \Delta_{\alpha} \delta_{\alpha\beta}$.

The single-particle Hamiltonian can be diagonalized as $\mathcal{G}_{\mathbf{k}\sigma}^{\dagger} \mathcal{H}_{\mathbf{k}\sigma} \mathcal{G}_{\mathbf{k}\sigma} = \epsilon_{\mathbf{k}\sigma}$. In this single-particle band basis, the field operators take the form

$$\begin{pmatrix} \mathbf{d}_{\mathbf{k}\uparrow} \\ \mathbf{d}_{\mathbf{q}-\mathbf{k}\downarrow}^{\dagger} \end{pmatrix} = \begin{pmatrix} \mathcal{G}_{\mathbf{k}\uparrow}^{\dagger} & 0 \\ 0 & \mathcal{G}_{\mathbf{q}-\mathbf{k}\downarrow}^{\dagger} \end{pmatrix} \Psi_{\mathbf{k}}, \quad (6)$$

where the components of the collective vector $(\mathbf{d}_{\mathbf{k}\uparrow}, \mathbf{d}_{\mathbf{q}-\mathbf{k}\downarrow}^{\dagger})^T$ correspond to different bands. A further unitary transformation to quasi-particle basis, $(\gamma_{\mathbf{k}, \mathbf{q}\uparrow}, \gamma_{\mathbf{k}, \mathbf{q}\downarrow}^{\dagger})^T$, diagonalizes the

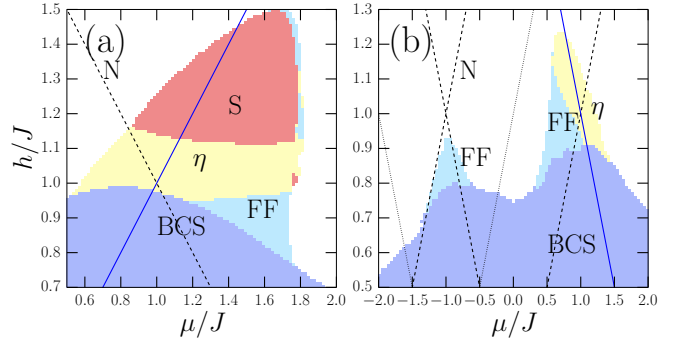


FIG. 2: Mean-field phase diagram for (a) a Lieb lattice and (b) kagome lattice at $U = -4J$ and $k_B T = 0.1J$. Here, $\mu = (\mu_{\uparrow} + \mu_{\downarrow})/2$ and $h = (\mu_{\uparrow} - \mu_{\downarrow})/2$. Dashed lines indicate Van Hove singularities, blue solid lines the FFs, and dotted lines the Dirac points. They are determined as $\mu_{\uparrow, \downarrow} = E_s$, i.e. where the chemical potential reaches the energy E_s corresponding to a relevant point in the DOS.

full BdG Hamiltonian, \mathcal{H}_{BdG} . The diagonalized Hamiltonian reads

$$H_{\text{FF}} = \sum_{\mathbf{k}} (\gamma_{\mathbf{k}, \mathbf{q}\uparrow}^{\dagger} \mathbf{E}_{\mathbf{k}, \mathbf{q}\uparrow} \gamma_{\mathbf{k}, \mathbf{q}\uparrow} + \gamma_{\mathbf{k}, \mathbf{q}\downarrow}^{\dagger} \mathbf{E}_{\mathbf{k}, \mathbf{q}\downarrow} \gamma_{\mathbf{k}, \mathbf{q}\downarrow}) + \mathcal{E}, \quad (7)$$

where $\mathbf{E}_{\mathbf{k}, \mathbf{q}\sigma}$ are diagonal matrices of the quasi-particle energies, and the energy offset $\mathcal{E} = \sum_{\mathbf{k}} (-3\mu_{\downarrow} + \text{Tr} \Delta^{\dagger} \Delta / U - \text{Tr} \mathbf{E}_{\mathbf{k}, \mathbf{q}\downarrow})$. In order to find thermodynamically stable phases at finite temperature, we look for global minima of the thermodynamic potential $\Omega = -\ln \text{Tr} \exp(-\beta H_{\text{FF}}) / \beta$, which can be calculated as

$$\Omega = -\frac{1}{\beta} \sum_{\mathbf{k}, \sigma} \text{Tr} \ln [1 + \exp(-\beta \mathbf{E}_{\mathbf{k}, \mathbf{q}\sigma})] + \mathcal{E}. \quad (8)$$

We minimize it with respect to all components of Δ and \mathbf{q} independently.

III. PHASE DIAGRAMS

We present mean field phase diagrams in Fig. 2 for both considered lattices, at interaction $U = -4J$ and temperature $k_B T = 0.1J$. Due to particle-hole symmetry, the phase diagram for the Lieb lattice is symmetric with respect to the axis $\mu = 0$. This symmetry is absent in the kagome lattice. We assume $\mu_{\uparrow} \geq \mu_{\downarrow}$. In both cases, the BCS phase is favored for sufficiently low chemical potential imbalance h . As h is increased, the phase switches either to a normal phase, or to nonuniform superfluidity with nonzero \mathbf{q} . We distinguish two such phases: the FF and η phase. In the FF region, \mathbf{q} is in the Brillouin zone (BZ) and grows until it reaches the boundary of the BZ. There, it saturates at its maximum value at the M point, $\mathbf{q} = (\pi, \pi)$ in the Lieb lattice and $\mathbf{q} = (0, \pi/\sqrt{3})$ in the kagome lattice. This means the order parameter oscillates with a period equal to twice the lattice period. This phase, otherwise similar to FFLO but with \mathbf{q} having such a maximal value, is referred to as the η phase in the literature^{42,43}. In the Lieb lattice, a third imbalanced superfluid phase with $\mathbf{q} = 0$,

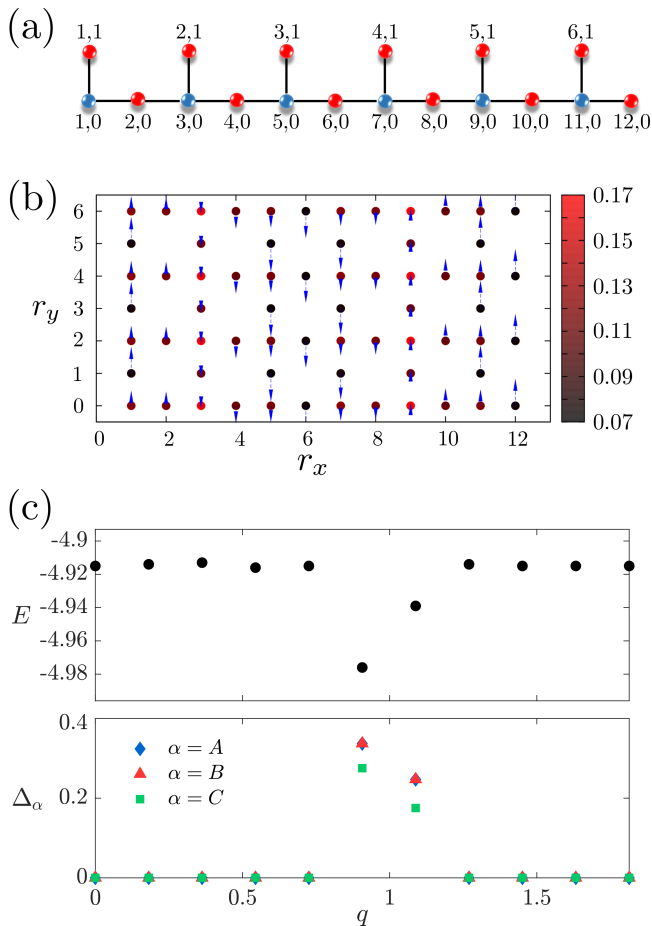


FIG. 3: (a) The 18 site cluster used for DMFT calculations for the Lieb lattice. (b) The s-wave order parameter, $\Delta(r_x, r_y)$ (arrow length and direction), and spin-polarization $n_s(r_x, r_y) = n_\uparrow(r_x, r_y) - n_\downarrow(r_x, r_y)$ (dots with color scale) for different positions (r_x, r_y) at $h \sim 1.40$, $\mu \sim 0.0$, $U = -6J$ and $k_B T = 0.05J$ in the FFLO state evaluated using DMFT for the Lieb lattice. (c) Total energy per unit cell (upper panel) and order parameters (lower panel) computed using DMFT, as a function of the amplitude of \mathbf{q} at lattice filling fractions $n_\uparrow \approx 2.06$ and $n_\downarrow \approx 1.62$ with $U = -4J$ and at zero temperature. In the lower panel, different symbols represent the order parameters in the three sites of the unit cell. In the FF state, two of the order parameters are equal due to the symmetry of the kagome lattice, while the third is smaller than the others due to the finite momentum \mathbf{q} , which breaks the symmetry of the lattice.

the so-called Sarma phase^{44–47}, is found at large imbalance h . The focus of this article is on the FF and η phases, and the Sarma phase will be discussed in detail in⁴⁸.

In both lattices, we find that the DOS singularities are manifested in the phase diagram. Nonuniform superfluidity occurs near crossing points of singularity lines, where the density of states near the FSs of both components is large. In the Lieb lattice, FB singularities are always involved at interaction $U = -4J$. In the kagome lattice, however, a smaller FF region is found away from the FB, where the minority component reaches the Van Hove (VH) singularity on the first dispersive band, and the majority component reaches that on the second

dispersive band.

Importantly, one can see from Fig. 2 that the FF and η phases are stable mostly close to the flat band DOS singularity. Near the flat band the FS of one component is small, or even nonexistent, and one would expect pairing to be suppressed. Indeed, in conventional BCS theory pairing is enhanced by the size of the FS. The formation of nonuniform superfluidity in our case is not explained solely by matching of the FSs as in previous literature³¹, indicating there are other mechanisms at play.

IV. DYNAMICAL MEAN-FIELD THEORY

To verify the existence of the FF phase beyond the simple mean-field approximation, we performed DMFT calculations in a partially real-space formulation for both lattices. Dynamical mean-field theory (DMFT) maps a lattice problem to an effective single impurity problem taking into account the lattice effects in a self-consistent manner. A central quantity is the self-energy $\Sigma_{ij}(i\omega_n)$, where i and j index the lattice sites and $\omega_n = \pi(2n+1)T$, where T is the temperature, are the fermionic Matsubara frequencies. Within single-site DMFT the self-energy is assumed to be local to each site i and uniform over the whole lattice, so that $\Sigma_{ij}(i\omega_n) \sim \delta_{ij}\Sigma(i\omega_n)$. For inhomogeneous states such as the Fulde-Ferrell-Larkin-Ovchinnikov phase (FFLO), however, the uniformity assumption breaks, as the order parameter can be different for different lattice sites. To study such states, we thus use a partially real-space cluster extension of DMFT^{64,65}, in which the self-energy is still local but varies spatially for different sites in the cluster, i.e. $\Sigma_{ij}(i\omega_n) = \Sigma_i(i\omega_n)\delta_{ij}$.

More rigorously, the DMFT method in Nambu-Gorkov formalism for a given cluster can be described as follows. The local Green's function of the lattice system limited to a single cluster can be calculated as

$$\mathbf{G}(i\omega_n) = \frac{1}{N_k} \sum_{\mathbf{k}} \left(\mathbf{G}^0(\mathbf{k}, i\omega_n)^{-1} - \Sigma(i\omega_n) \right)^{-1}, \quad (9)$$

where the bold quantities are matrices whose dimension equals the number of sites within the cluster and N_k is the number of k -points. Each component consists of a (2×2) matrix with normal Green's functions as diagonal components, while the off-diagonal components are anomalous Green's functions. Thus the 2×2 block $\mathbf{G}(i\omega_n)_{ij}$ is the Green's function between sites i and j of the cluster. The non-interacting Green's function $\mathbf{G}^0(\mathbf{k}, i\omega_n)_{ij}^{-1} = (i\omega_n + h)\delta_{ij}\sigma_0 + \mu\delta_{ij}\sigma_z - \mathbf{T}(\mathbf{k})_{ij}\sigma_z$, where $\mathbf{T}(\mathbf{k})$ is the superlattice Fourier transform of the hopping matrix. The site diagonal self-energy at the i th site is given by the following (2×2) matrix

$$\Sigma_i(i\omega_n) = \begin{pmatrix} \Sigma_i(i\omega_n) & S_i(i\omega_n) \\ S_i(i\omega_n) & -\Sigma_i^*(i\omega_n) \end{pmatrix}$$

where $\Sigma(i\omega_n)$ ($S(i\omega_n)$) is the normal (anomalous) part of the self-energy. For each site i in the cluster, there is an effective single impurity Anderson model, which is defined by the dynamical Weiss mean-field

$$\mathcal{G}_i(i\omega_n)^{-1} = (\mathbf{G}(i\omega_n)_{ii})^{-1} + \Sigma_i(i\omega_n). \quad (10)$$

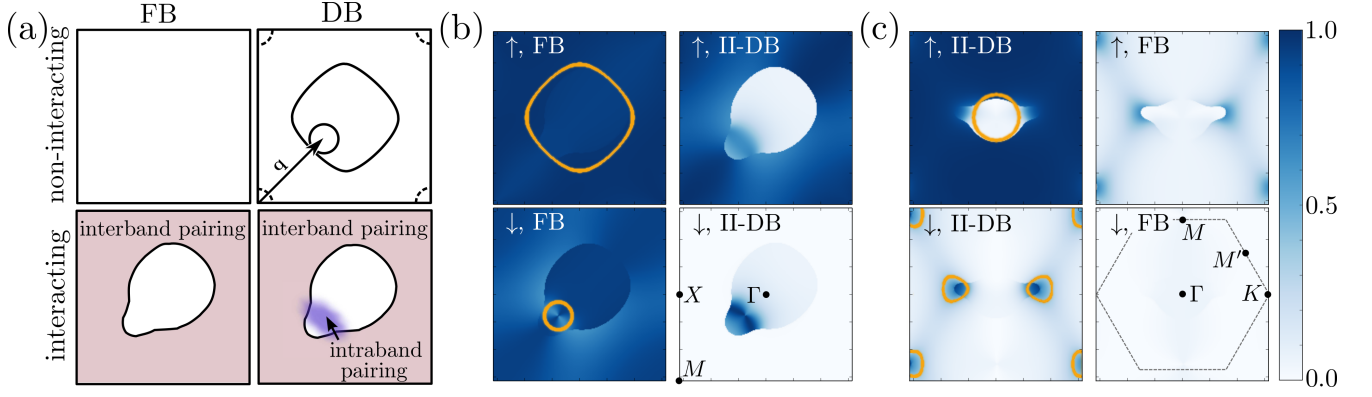


FIG. 4: (a) The FF pairing mechanism in a multiband system with a FB. The FS of the minority component shifts towards the FS of the majority component by the momentum \mathbf{q} . Both intra- and interband pairings (regions which are shown here in color) contribute to the overall effect. The calculated band-resolved density profiles $n_{\mathbf{k}\sigma}$ in (b) the Lieb lattice for $\mu = 1.4J$ and $h = 0.9J$ and in (c) the kagome lattice for $\mu = 0.6J$ and $h = 1.1J$ demonstrate the discussed scenario. Orange lines indicate the noninteracting Fermi surfaces. High-symmetry points are marked, and dashed lines in (c) indicate the boundary of the Brillouin zone.

Given the Weiss function \mathcal{G}_i for all i , we calculate the self-energy of each of the impurity problems using a continuous time quantum Monte-Carlo (CTINT) algorithm⁶⁶ for the Lieb lattice, and an exact diagonalization (ED) solver for the kagome lattice. These new self-energies are then used again in equation 9 and the process is iterated until a converged solution is found.

For the Lieb lattice, the calculations were performed for a cluster of 18 sites, shown in Fig. 3. At half-filling, it is expected that the three-site unit cell (see Fig. 1) is sufficient to investigate the interaction-induced order parameters, while larger clusters should be considered to capture FFLO order appearing in the spin-imbalanced case. Further we define the s-wave order parameter from the anomalous Green's function F as

$$\Delta(r_x, r_y) = UF(r_x, r_y)(\tau \rightarrow 0^-) \quad (11)$$

where (r_x, r_y) are the positions of the sites in the unit cell and τ is the imaginary time. Similarly, we denote $n_\sigma(r_x, r_y) = G(r_x, r_y, \sigma)(\tau \rightarrow 0^-)$, where G is the normal Green's function and σ is the spin degree of freedom, and define the spin-polarization as

$$n_s(r_x, r_y) = n_\uparrow(r_x, r_y) - n_\downarrow(r_x, r_y). \quad (12)$$

The two dimensional profile distribution of the s-wave order parameter, $\Delta(r_x, r_y)$, and spin-polarization, $n_s(r_x, r_y) = n_\uparrow(r_x, r_y) - n_\downarrow(r_x, r_y)$, in the Lieb lattice are shown in Fig. 3. In the figure, the 18-site cluster is stacked in the y -direction. The modulations of the order parameter and spin-polarization are a clear indication of an FFLO state.

In the kagome lattice, calculations were performed on the three-site unit cell shown in Fig. 1 in the main text. The Fulde-Ferrell (FF) ansatz $\Delta_{\mathbf{j}\alpha} = \Delta_\alpha e^{i\mathbf{q}\cdot\mathbf{j}}$ is included by performing the transformation $\psi_{\mathbf{j}\alpha\uparrow} \rightarrow \psi_{\mathbf{j}\alpha\uparrow} e^{-i\mathbf{q}\cdot\mathbf{r}_j}$, where \mathbf{r}_j is the position of the j th lattice site. The dependence on the momentum \mathbf{q} of the Cooper pairs is then included in the hopping matrices, and the non-interacting Green's function becomes $\mathbf{G}^0(\mathbf{k}, i\omega_n)_{ij}^{-1} =$

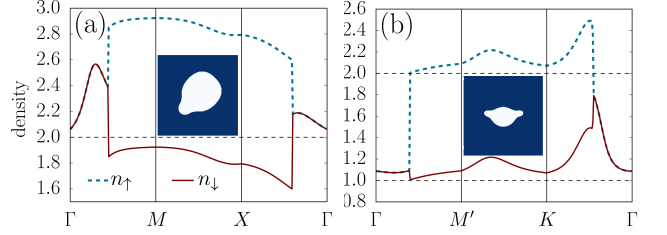


FIG. 5: Densities along high symmetry symmetry lines in (a) the Lieb and (b) the kagome lattice. Coinciding densities indicate complete pairing, whereas a jump in density $n_{\mathbf{k}\uparrow} - n_{\mathbf{k}\downarrow} = 1$ arises due to the presence of a normal gas characteristic for spin-imbalanced superfluids. The region where this unpaired component resides is shown as insets. Dark blue (white) corresponds to a value of one (zero) of $n_{\mathbf{k}\uparrow} - n_{\mathbf{k}\downarrow}$.

$(i\omega_n + h)\delta_{ij}\sigma_0 + \mu\delta_{i,j}\sigma_0 - \text{diag}(\mathbf{T}(\mathbf{k} - \mathbf{q})_{ij}, -\mathbf{T}(\mathbf{k})_{ij})$, where $\mathbf{T}(\mathbf{k})$ is again the Fourier transform of the hopping matrix. Like in the Lieb lattice, the self-energy is assumed local, but can be different for the three sites in the unit cell.

The computation for the kagome lattice is performed at different amplitudes of \mathbf{q} , with the direction fixed perpendicular to one of the lattice vectors, corresponding to the most favorable direction found in mean-field calculations. The chemical potentials are tuned to achieve the same filling fractions for all different \mathbf{q} , and the most favorable amplitude is determined by comparing the total energies. The results for lattice filling fractions $n_\uparrow \approx 2.06$ and $n_\downarrow \approx 1.62$ with interaction $U = -4J$, are shown in Fig. 3. The computation converged to a state with finite order parameters around $q \approx 1.0$, indicating an FF state. The FF state at $q \approx 0.73$ gave the lowest total energy. At these filling fractions, the majority component has reached the flat band, so these results confirm the mean-field observation that the FF state can exist near the flat-band singularity.

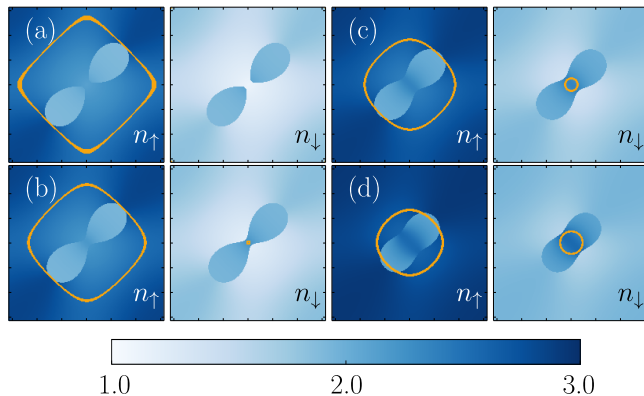


FIG. 6: (a) Total densities of each spin component for four different parameters. The shape of the deformed Fermi surface is revealed by the distribution of the normal part, as it changes within the η phase as we move away from the crossing of the flat band and the Van Hove singularity, i.e. along the line of $h = 1.05J$; Subsequent panels are for (a) $\mu = J$, (b) $\mu = 1.1J$, (c) $\mu = 1.3J$, (d) $\mu = 1.5J$. Since the I-DB is completely filled, the color scale was truncated to the range from 1 to 3.

V. PAIRING MECHANISM

In order to get an insight into the mechanism of pairing in these multiband systems, we look at the band resolved densities, $n_{\mathbf{k}n\sigma} = \langle d_{\mathbf{k}n\sigma}^\dagger d_{\mathbf{k}n\sigma} \rangle$, where n is the band index, that is, densities of each spin component decomposed in the band basis of the single-particle Hamiltonian. As presented in the schematic in Fig. 4(a), we find that the FS of the minority component gets shifted by a vector \mathbf{q} towards the Fermi surface of the majority component where the pairing takes place — this is the conventional mechanism behind the FFLO state^{14,15,31}. In a square lattice, this leads to nesting which stabilizes the FFLO state^{28,31}. In our case this is *intra*-band pairing, i.e. pairing between atoms from the same band, as will be explained later. The calculated band-resolved densities are shown in Fig. 4(b) for the Lieb lattice and in Fig. 4(c) for the kagome lattice. The lower dispersive band (I-DB) remains almost completely filled (and therefore we do not plot it), while deformation of the density distributions takes place in the upper dispersive band (II-DB) in the region where the FSs match.

An interesting effect can be observed for atoms residing in the FB. For one component they remain completely unaffected, while for the other the distribution of atoms, which was initially flat, gets deformed in such a way as to mimic the density of the first component in the II-DB. In the case of a Lieb lattice (kagome lattice) the FB remains completely filled (completely empty) for the majority (minority) component, while for the minority (majority) component the distribution of atoms gets deformed. This suggests an *inter*-band pairing between the atoms in the FB and atoms in the II-DB. This is an energetically favorable process, as the atoms in a FB can rearrange at vanishing energy cost due to flat dispersion relation. Such density rearrangement without energy cost is the key physical role of the FB in enhancing exotic pairing.

The excess atoms of the majority component, that do not

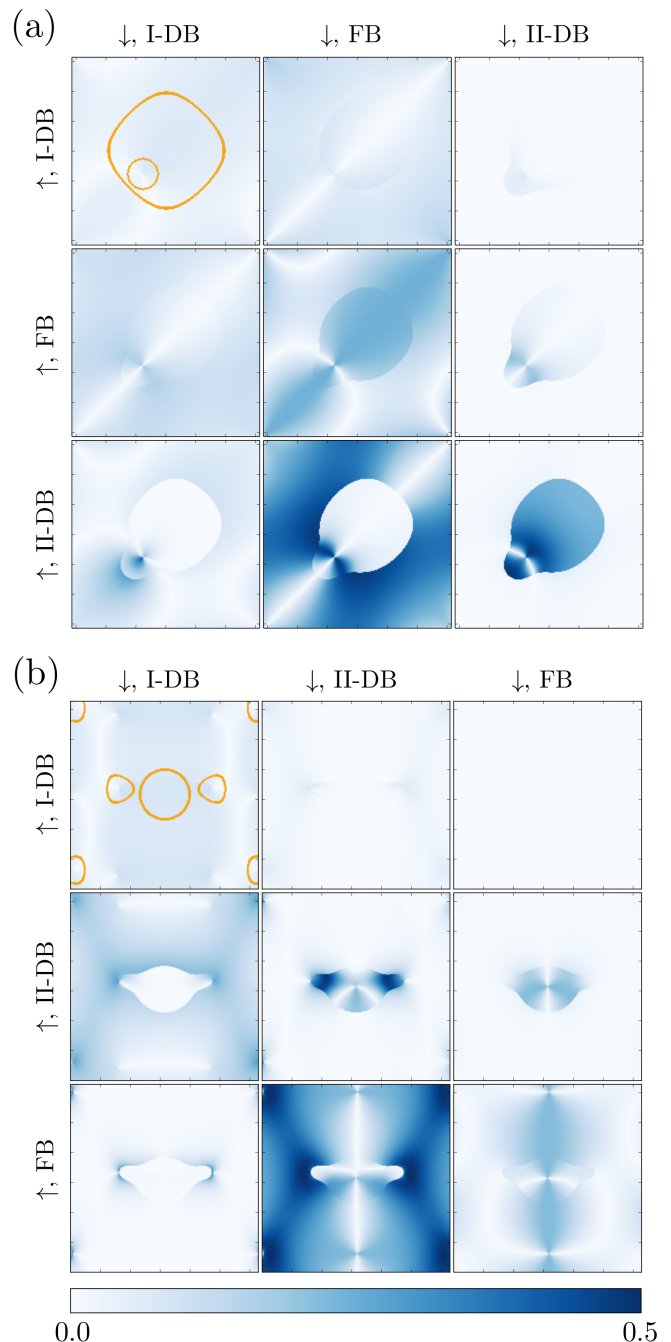


FIG. 7: Pairing $\langle d_{\mathbf{k}n\uparrow} d_{(\mathbf{q}-\mathbf{k})m\downarrow} \rangle$ between different bands in (a) the Lieb lattice and (b) the kagome lattice at the parameters used in Fig. 4. Most pairing takes place as intraband pairing in the II-DB and as interband pairing between the FB and the II-DB.

take part in the pairing, form a normal gas. Its presence can be seen in the total density traced along the high-symmetry lines, as well as in the differences $n_{\mathbf{k}\uparrow} - n_{\mathbf{k}\downarrow}$, as shown in Fig. 5 for both lattices. The density profiles of the paired components are matched up to a shift by a constant; for some momenta \mathbf{k} there is a jump in the densities of the two components. This is due to the presence of a normal gas. Since, as is stated by Luttinger's theorem, the number of available states inside the

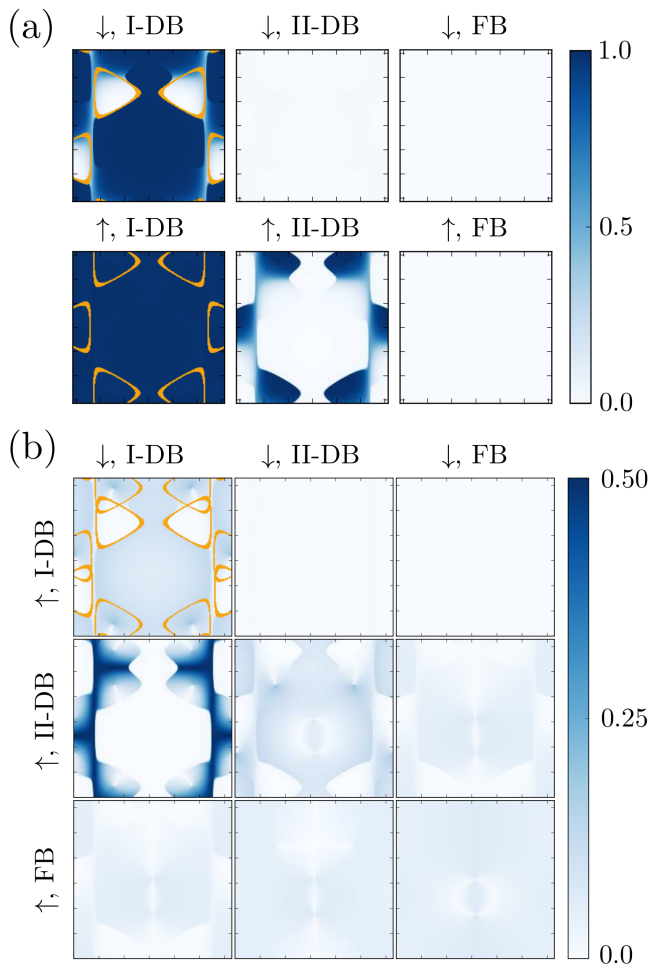


FIG. 8: (a) Band-resolved density profiles and (b) pairing $\langle d_{\mathbf{k}\uparrow} d_{(\mathbf{q}-\mathbf{k})\downarrow} \rangle$ in the kagome lattice at $\mu = -1.0$, $h = 0.9$, $U = -4J$ and $T = 0$. The pairing is mainly interband pairing between the two dispersive bands, and correlations are most pronounced where the Fermi surfaces of the two components are matched.

Fermi sphere does not change upon interactions, this constant shift is $n_{\mathbf{k}\uparrow} - n_{\mathbf{k}\downarrow} = 1$, see Ref.³¹. This mechanism can be seen also in the band-resolved densities in Figs. 4(a), (b). The presence of the normal gas in the upper dispersive band gives rise to an observable FS seen as sharp density jumps. Even though the normal component does not participate in the pairing, its Fermi surface is deformed by the pairing mechanism of the other atoms.

As we approach the flat band singularity within the η phase in the phase diagram of the Lieb lattice, the deformation of the Fermi surface becomes more and more pronounced. This deformation is such that there be as large a matching as possible between the two FSs. That is where most of the intraband pairing takes place. In Fig. 6 we show four examples of cumulative density for each spin component along the line of $h = 1.05J$. When one of the non-interacting FSs vanishes at the Dirac point, the deformation is the most dramatic, and the continuity of the FS is broken.

To gain further understanding of the nature of pair-

ing, we study pairing correlations between different bands, $\langle d_{\mathbf{k}\uparrow} d_{(\mathbf{q}-\mathbf{k})\downarrow} \rangle$, where n and m are band indices. As can be seen in Figs. 7(a),(b), the lattices feature both intra- and interband pairing. Intraband pairing occurs mostly between particles on II-DB, and is most pronounced in the region where the Fermi surfaces match. This is similar to what is found in the square lattice, where particles on the same energy band can pair due to the shift of one FS by \mathbf{q} . The Fermi surface of the normal component is reflected also in the pairing correlations, and intraband pairing within II-DB is completely absent in the region where the unpaired particles reside. The other prominent pairing is between particles on the FB and those on II-DB. Again, the FS of the normal component is visible as sharp jumps between low and high correlations. Contrary to intraband pairing, this interband pairing occurs mostly where the unpaired gas lies, and the paired components occupy different energy bands. Pairing is made possible in this situation by the possibility of atoms on the FB to readjust their density profile to mimic that of the other component on II-DB at low energy cost.

Correlations between other bands, albeit smaller, are also present. In particular, also particles of the majority (minority) component on the FB contribute to pairing in the Lieb (kagome) lattice. Moreover, the various pairings give further indication that the unpaired particles are distributed among different bands.

To better understand the effect of the flat band, it is instructive to compare the pairing mechanisms in the FF phase near the FB singularity to those in the other FF region found for the kagome lattice. As can be seen from the band-resolved densities and correlations shown in Fig. 8, the FB is almost empty for both components, and contributes little to the pairing. The dominant pairing is interband between atoms on the first and second dispersive bands. Interestingly, even though the Fermi surfaces are perfectly matched at zero \mathbf{q} , the FF phase is favorable. This is due to the different distributions of the components: the minority component occupies the center of the BZ, whereas the majority component occupies the corners. The momentum \mathbf{q} allows for the Fermi seas of the two components to overlap slightly, increasing the number of states near the Fermi surface that can pair.

The comparison with pairing correlations near the FB highlights the effect of a FB on the pairing mechanism. Intraband pairing is almost absent in the FF region away from the flat band, whereas both intra- and interband pairings are found near the FB singularity. Moreover, the possibility for atoms on the FB to rearrange allows for pairing to occur in a large region of the BZ, instead of being limited to the comparatively small region where Fermi surfaces are matched.

The pairing correlations in the band basis for the η phase at the flat band (near the point where the singularities cross) show the same mechanism as described for the generic FF phase: in the Lieb lattice intraband pairing is mostly concentrated within the II-DB and within the flat band, and the interband pairing between the flat band and the II-DB. The difference is that the deformed FS in the η phase is symmetric with respect to the Γ point; this is due to the four-fold symmetry of the original, non-interacting FSs.

VI. EXPERIMENTAL PROSPECTS

While other possibilities also exist^{37–41}, ultracold quantum gases may offer the most immediate realization of our predictions. Lieb and kagome geometries have already been realized by optical lattices^{34–36} and novel techniques such as digital mirror devices and holograms^{49–51} allow further flexibility. Our mean-field calculations give critical temperatures $k_B T_c$ from around $0.2 J$ to $0.5 J$ ⁴⁸. In 2D, the Berezinskii-Kosterlitz-Thouless (BKT) temperature for superfluidity is typically smaller than the BCS one but can be of the same order of magnitude^{52–54}. Deformations and nontrivial pairing correlations may appear in these flat band systems already well above the critical temperature, which is an interesting topic of future study.

VII. CONCLUSIONS

In summary, we studied the attractive Hubbard model on the Lieb and kagome lattices, both featuring a FB. We found a stable FFLO phase, present due to inter- and intraband pairings that involve the FB. This mechanism of spin-imbalanced pairing relies on complete deformation of the density of one pairing component, enabled by the FB, and is therefore strik-

ingly different from the conventional minority FS shift (and nesting in lattices). Flat band singularities are known to enhance magnetism^{55–57} and superfluidity^{52–54,58–62}; here we have shown that, in the case of spin-imbalanced pairing, not only does it enhance interactions, but also it makes the pairing mechanism qualitatively different. Since experimental preparation of artificial lattice quantum systems is advancing rapidly^{8,38,63}, our predictions may show the route to direct observation of spin-imbalanced pairing and superfluidity.

VIII. ACKNOWLEDGMENTS

This work was supported by the Academy of Finland through its Centres of Excellence Programme (2012-2017) and under project NOs. 284621, 303351 and 307419, and by the European Research Council (ERC-2013-AdG-340748-CODE). This project has received funding from the European Unions Horizon 2020 research and innovation programme under the Marie Skłodowska-Curie Grant Agreement No. 702281 (FLATOPS). T.I.V. acknowledges support from the Väisälä foundation. Computing resources were provided by CSC – the Finnish IT Centre for Science and the Triton cluster at Aalto University.

-
- ¹ L. N. Cooper, *Phys. Rev.* **104**, 1189 (1956).
² I. I. Pomeranchuk, *JETP* **8**, 361 (1959).
³ J. G. Bednorz and K. A. Müller, *Zeitschrift für Physik B Condensed Matter* **64**, 189 (1986).
⁴ P. A. Lee, N. Nagaosa, and X.-G. Wen, *Rev. Mod. Phys.* **78**, 17 (2006).
⁵ I. Bloch, J. Dalibard, and W. Zwerger, *Rev. Mod. Phys.* **80**, 885 (2008).
⁶ M. Sato and Y. Ando, *Reports on Progress in Physics* **80**, 076501 (2017).
⁷ A. J. Leggett, *Rev. Mod. Phys.* **47**, 331 (1975).
⁸ P. Törmä and K. Sengstock, *Quantum Gas Experiments: Exploring Many-Body States* (World Scientific Publishing Co, 2015).
⁹ M. Iskin, *Phys. Rev. A* **88**, 013631 (2013).
¹⁰ C. Qu, Z. Zheng, M. Gong, Y. Xu, L. Mao, X. Zou, G. Guo, and C. Zhang, *Nature Communications* **4**, 2710 (2013).
¹¹ T. I. Vanhala and P. Törmä, ArXiv e-prints (2017), arXiv:1708.06749.
¹² M. L. Kiesel, C. Platt, and R. Thomale, *Phys. Rev. Lett.* **110**, 126405 (2013).
¹³ M. Kitatani, N. Tsuji, and H. Aoki, *Phys. Rev. B* **95**, 075109 (2017).
¹⁴ P. Fulde and R. A. Ferrell, *Phys. Rev.* **135**, A550 (1964).
¹⁵ A. Larkin and Y. Ovchinnikov, *JETP* **20**, 762 (1965).
¹⁶ H. Mütter and A. Sedrakian, *Phys. Rev. Lett.* **88**, 252503 (2002).
¹⁷ A. Sedrakian, J. Mur-Petit, A. Polls, and H. Mütter, *Phys. Rev. A* **72**, 013613 (2005).
¹⁸ R. Casalbuoni and G. Nardulli, *Rev. Mod. Phys.* **76**, 263 (2004).
¹⁹ Y.-a. Liao, A. S. C. Rittner, T. Paprotta, W. Li, G. B. Partridge, R. G. Hulet, S. K. Baur, and E. J. Mueller, *Nature* **467**, 567 EP (2010).
²⁰ M. W. Zwierlein, A. Schirotzek, C. H. Schunck, and W. Ketterle, *Science* **311**, 492 (2006).
²¹ G. B. Partridge, W. Li, R. I. Kamar, Y.-a. Liao, and R. G. Hulet, *Science* **311**, 503 (2006).
²² G. B. Partridge, W. Li, Y. A. Liao, R. G. Hulet, M. Haque, and H. T. C. Stoof, *Phys. Rev. Lett.* **97**, 190407 (2006).
²³ Y. Shin, C. H. Schunck, A. Schirotzek, and W. Ketterle, *Nature* **451**, 689 (2008).
²⁴ S. Nascimbène, N. Navon, K. J. Jiang, L. Tarruell, M. Teichmann, J. McKeever, F. Chevy, and C. Salomon, *Phys. Rev. Lett.* **103**, 170402 (2009).
²⁵ D. E. Sheehy and L. Radzihovsky, *Phys. Rev. Lett.* **96**, 060401 (2006).
²⁶ D. E. Sheehy and L. Radzihovsky, *Annals of Physics* **322**, 1790 (2007).
²⁷ A. Recati, C. Lobo, and S. Stringari, *Phys. Rev. A* **78**, 023633 (2008).
²⁸ T. K. Koponen, T. Paananen, J.-P. Martikainen, and P. Törmä, *Phys. Rev. Lett.* **99**, 120403 (2007).
²⁹ M. J. Wolak, B. Grémaud, R. T. Scalettar, and G. G. Batrouni, *Phys. Rev. A* **86**, 023630 (2012).
³⁰ J. E. Baarsma and P. Törmä, *Journal of Modern Optics* **63**, 1795 (2016).
³¹ J. J. Kinnunen, J. Baarsma, J.-P. Martikainen, and P. Törmä, *Reports on Progress in Physics* (also arXiv:1706.07076) (2018).
³² A. Cichy and A. Ptok, ArXiv e-prints (2017), arXiv:1710.06395.
³³ M. O. J. Heikkinen, D.-H. Kim, M. Troyer, and P. Törmä, *Phys. Rev. Lett.* **113**, 185301 (2014).
³⁴ G.-B. Jo, J. Guzman, C. K. Thomas, P. Hosur, A. Vishwanath, and D. M. Stamper-Kurn, *Phys. Rev. Lett.* **108**, 045305 (2012).
³⁵ S. Taie, H. Ozawa, T. Ichinose, T. Nishio, S. Nakajima, and Y. Takahashi, *Science Advances* **1** (2015), 10.1126/sci-

- adv.1500854.
- ³⁶ H. Ozawa, S. Taie, T. Ichinose, and Y. Takahashi, *Phys. Rev. Lett.* **118**, 175301 (2017).
- ³⁷ M. R. Slot, T. S. Gardenier, P. H. Jacobse, G. C. P. van Miert, S. N. Kempkes, S. J. M. Zevenhuizen, C. M. Smith, D. Vanmaeckelbergh, and I. Swart, *Nat Phys* **13**, 672 (2017).
- ³⁸ R. Drost, T. Ojanen, A. Harju, and P. Liljeroth, *Nat Phys* **13**, 668 (2017).
- ³⁹ S. Mukherjee, A. Spracklen, D. Choudhury, N. Goldman, P. Öhberg, E. Andersson, and R. R. Thomson, *Phys. Rev. Lett.* **114**, 245504 (2015).
- ⁴⁰ R. A. Vicencio, C. Cantillano, L. Morales-Inostroza, B. Real, C. Mejía-Cortés, S. Weimann, A. Szameit, and M. I. Molina, *Phys. Rev. Lett.* **114**, 245503 (2015).
- ⁴¹ X.-H. Deng, C.-Y. Lai, and C.-C. Chien, *Phys. Rev. B* **93**, 054116 (2016).
- ⁴² C. N. Yang, *Phys. Rev. Lett.* **63**, 2144 (1989).
- ⁴³ A. Ptok, A. Cichy, K. Rodríguez, and K. J. Kapcia, *Phys. Rev. A* **95**, 033613 (2017).
- ⁴⁴ G. Sarma, *J. Phys. Chem. Solids* **24**, 1029 (1963).
- ⁴⁵ W. V. Liu and F. Wilczek, *Phys. Rev. Lett.* **90**, 047002 (2003).
- ⁴⁶ L. He and P. Zhuang, *Phys. Rev. B* **79**, 024511 (2009).
- ⁴⁷ D.-H. Kim, J. S. J. Lehtikoinen, and P. Törmä, *Phys. Rev. Lett.* **110**, 055301 (2013).
- ⁴⁸ M. Tylutki and P. Törmä, to be published (2018).
- ⁴⁹ K. Hueck, A. Mazurenko, N. Luick, T. Lompe, and H. Moritz, *Review of Scientific Instruments* **88**, 016103 (2017), <https://doi.org/10.1063/1.4973969>.
- ⁵⁰ G. Gauthier, I. Lenton, N. M. Parry, M. Baker, M. J. Davis, H. Rubinsztein-Dunlop, and T. W. Neely, *Optica* **3**, 1136 (2016).
- ⁵¹ P. Zupancic, P. M. Preiss, R. Ma, A. Lukin, M. E. Tai, M. Rispoli, R. Islam, and M. Greiner, *Opt. Express* **24**, 13881 (2016).
- ⁵² S. Peotta and P. Törmä, *Nat. Comm.* **6**, 8944 (2015).
- ⁵³ A. Julku, S. Peotta, T. I. Vanhala, D.-H. Kim, and P. Törmä, *Phys. Rev. Lett.* **117**, 045303 (2016).
- ⁵⁴ L. Liang, T. I. Vanhala, S. Peotta, T. Siro, A. Harju, and P. Törmä, *Phys. Rev. B* **95**, 024515 (2017).
- ⁵⁵ A. Mielke, *Journal of Physics A: Mathematical and General* **25**, 4335 (1992).
- ⁵⁶ H. Tasaki, *Phys. Rev. Lett.* **69**, 1608 (1992).
- ⁵⁷ A. Mielke and H. Tasaki, *Comm. Math. Phys.* **158**, 341 (1993).
- ⁵⁸ V. A. Khodel and V. R. Shaginyan, *JETP* **51**, 553 (1990).
- ⁵⁹ V. Khodel, V. Shaginyan, and V. Khodel, *Physics Reports* **249**, 1 (1994).
- ⁶⁰ T. T. Heikkilä, N. B. Kopnin, and G. E. Volovik, *JETP Letters* **94**, 233 (2011).
- ⁶¹ N. B. Kopnin, T. T. Heikkilä, and G. E. Volovik, *Phys. Rev. B* **83**, 220503 (2011).
- ⁶² D. Yamamoto, C. Sato, T. Nikuni, and S. Tsuchiya, *Phys. Rev. Lett.* **110**, 145304 (2013).
- ⁶³ S. Kuhr, *National Science Review* **3**, 170 (2016).
- ⁶⁴ P. Kumar, T. I. Vanhala, and P. Törmä, *Phys. Rev. B* **96**, 245127 (2017).
- ⁶⁵ T. Maier, M. Jarrell, T. Pruschke, and M. H. Hettler, *Rev. Mod. Phys.* **77**, 1027 (2005).
- ⁶⁶ E. Gull, A. J. Millis, A. I. Lichtenstein, A. N. Rubtsov, M. Troyer, and P. Werner, *Rev. Mod. Phys.* **83**, 349 (2011).